Analysis of drill-bit data: preliminary results

Clement Kostov and Luigi Zanzi

ABSTRACT

The concept of an experiment using the drill-bit signal as a downhole seismic source is presented. The first step in the processing of data from such experiments is to separate the drill-bit signal from the noise generated by surface sources; then a variety of applications taking advantage of the source location can be considered. We discuss methods for the analysis of the temporal and spatial characteristics of drill-noise data; the application of these methods to field data from a preliminary field survey allow us to identify strong narrow-band sources of noise at the surface.

INTRODUCTION

The goal of our project is to develop signal processing techniques capable of using the signal generated by the drill-bit as a downhole seismic source.

The field experiment is relatively simple – an array of geophones on the surface records ambient noise during the drilling operation. In addition, geophones or strong motion sensors could monitor noise generated by equipment on the surface.

The most attractive feature of the drill-bit as a source of seismic signal is that it operates continuously as a downhole source. On the other hand, intensive signal processing is necessary to separate the drill-bit signal from the noise generated by strong and spatially coherent sources. Then, depending on the bandwidth of the signal from the drill-bit, a variety of goals and processing schemes could be considered.

Field data from a survey, where the depth of the well is less than 100m will be presented below. These data are interesting mainly for the information provided about the sources of noise at the surface. In the week before the report deadline, we received at SEP two additional datasets for wells with depths up to 1.5km. The new data should allow to evaluate the methods for separation of drill-bit signal from surface noise in a more favorable situation.

In the first section we discuss general approaches to the processing of drill-bit data. Then we describe the acquisition parameters for the shallow-well experiment. In the third and fourth sections we comment the results of our analysis of the drill-bit data – spectral content and velocity analysis.

SEPARATING THE DRILL-BIT SIGNAL FROM NOISE

The drill-bit is neither the only, nor the strongest acoustic source near a drill-site. Sources of noise include the equipment on the surface, such as pumps and generators, equipment in the borehole, and traffic near the rig. Tube waves, that have high amplitude in the borehole, could also generate by conversion at the free-surface both surface and body waves that propagate at significant distances away from the borehole (Samec and Kostov, SEP-57).

The initial model for the data recorded at the array of geophones is a superposition of the fields of several sources. To estimate the parameters describing a planar, or, a spherical wavefront impinging on an array of geophones we apply methods for beamforming described elsewhere in this report in the contexts of passive seismology by Cole, (SEP-57), and of velocity analysis by Biondi and Kostov, (SEP-57). Once the parameters of a wavefront are estimated, filters can be designed to separate the desired wavefront from the other data (Cassano and Rocca, 1973), (Harlan et al., 1984). Suppression of dominant sources and estimation of parameters of weaker ones may be repeated until the signal from the drill-bit is identified on the basis of the approximately known location of the drill-bit.

Prior knowledge of some parameters of the sources will help the separation of signal from noise. Therefore, geophones can be used to monitor the noise from the equipment at the surface. A strong motion sensor on the drill-rig might provide a record that is highly correlated with the drill-bit signal. Also, some of the mechanical installations at the surface are easily identifiable from their spectra, concentrated at a few harmonic lines. Further understanding of the experiment will help to develop a model for the characteristics of the drill-bit signal – radiation pattern, bandwidth, and variability in time.

THE SHALLOW-WELL SURVEY

A sketch of the layout of the geophones is shown in Figure 1. The geophones are arranged in two perpendicular lines, with 30 channels each. The spacing between channels is 10 m; the near offset is 20m on the EW line, and 30 m on the NS line. The geophones are arranged in groups of six along circumferences of diameter 0.6m. The well is off the center of the lines; the farthest offset is 210m. The length of the lines is consistent with the shallow depth of the well.

Ambient noise was recorded during 103 periods of 10sec each; the sampling interval in time is 2 msec. Half of the gathers are recorded for depths of the drill-

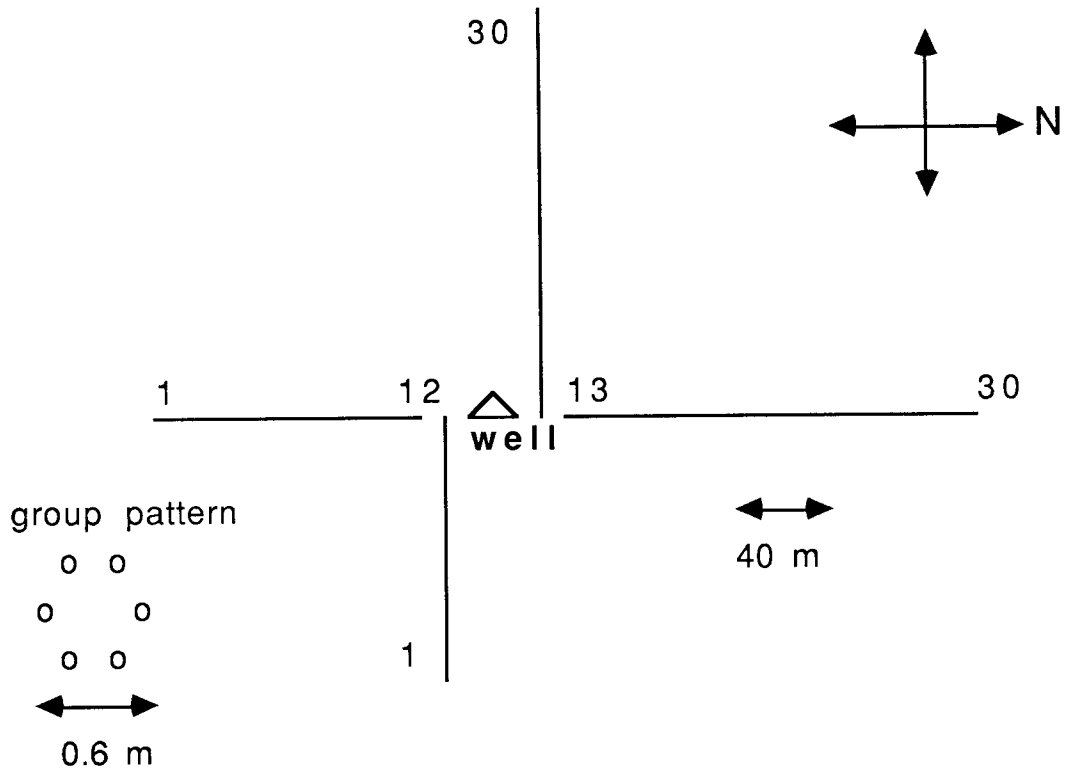

FIG. 1. Sketch of the relative positions of the well and of the two seismic lines during the shallow-well experiment. There are 30 channels in each line. The well is in the axis of the NS line, and off-axis for the EW line. Geophones are arranged in groups along a circumference of diameter 0.6m.

bit between 50 and 56m; for the other half of the gathers the depth of the tool is between 80 and 85m. Frequencies above 128 Hz are high-cut filtered during the recording.

Aliasing in space of the wavefronts arriving on the array will occur when

$$k_x \geq \frac{1}{2\Delta x} = k_{Nyq},$$

where k_x is the horizontal component of the wave-vector, $\Delta x = 10$m is the spacing between channels, and k_{Nyq} is the Nyquist wavenumber. In terms of frequency ω and velocity v, the above condition becomes:

$$v \geq \frac{\omega \sin(\theta)}{k_{Nyq}} = 20.\omega \sin(\theta),$$

with θ being the angle between the wave-vector $\mathbf{k}$ and a line perpendicular to the array. For instance, when the depth of the drill-bit is 50m, θ varies from 22° at near

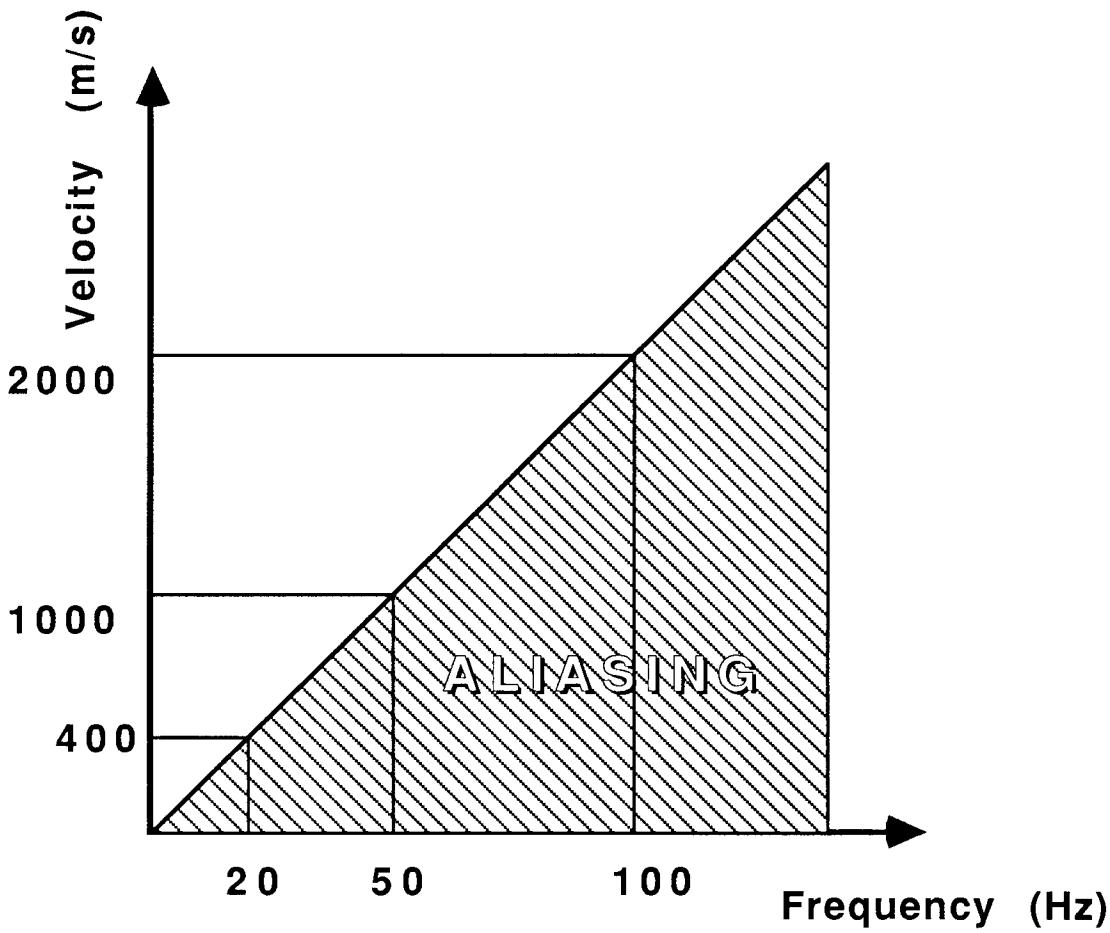

FIG. 2. The frequency and the velocity below which spatial aliasing occurs are linearly related. The plot shows the relationship for far offsets and for depth of the drill-bit of 50m.

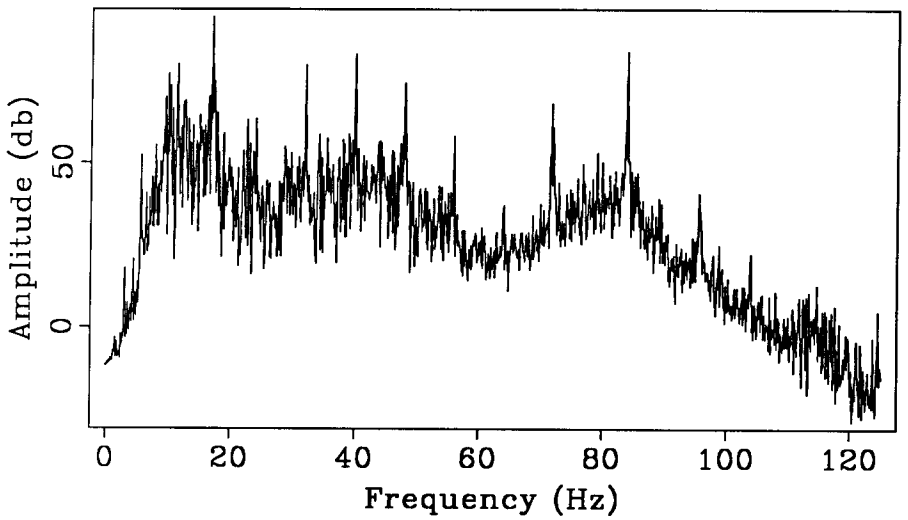

FIG. 3. Spectrum of drill bit data; average of the spectra of the 30 traces within a gather. Each trace is 10 sec long, sampled at 4 msec. The spectra are computed by applying the Discrete Fourier Transform, without smoothing in the frequency domain, or averaging over time. The scale is logarithmic, in decibels (db).

offset to 74° at far offsets. Then, waves traveling at velocities less than 800 m/sec will be aliased at far offsets for all frequencies greater than 40 Hz.

The location of the pumps, generators, mud reservoirs, and other equipment was not indicated on the map, and there were no geophones monitoring the signal either from these installations or from the drill-rig.

SPECTRAL ANALYSIS

In this section we analyze the properties of the frequency spectra of the data from the shallow-well survey. We display first the variations of the spectra as a function of the recording period, and second, measure the variability in time of the signal within a recording period of 10 sec.

Variations of the spectra with recording period

A typical spectrum of drill-bit data is shown in Figure 3. Strong spectral lines, more than 30db above the background, appear clearly.

The spectra of signals with strong line components are best estimated by introducing a parametric model for the signal. The spectrum in Figure 3 has no deep notches, therefore we choose an auto-regressive model for the signal, i.e. the signal is obtained as the convolution of a white noise process with an all-pole filter. The optimal filter of a given length may be obtained by one of several algorithms, including the Burg algorithm (Marple, 1987), (Claerbout, 1985). The spectrum computed by the Burg algorithm with 400 poles, is shown for comparison in Figure 4.

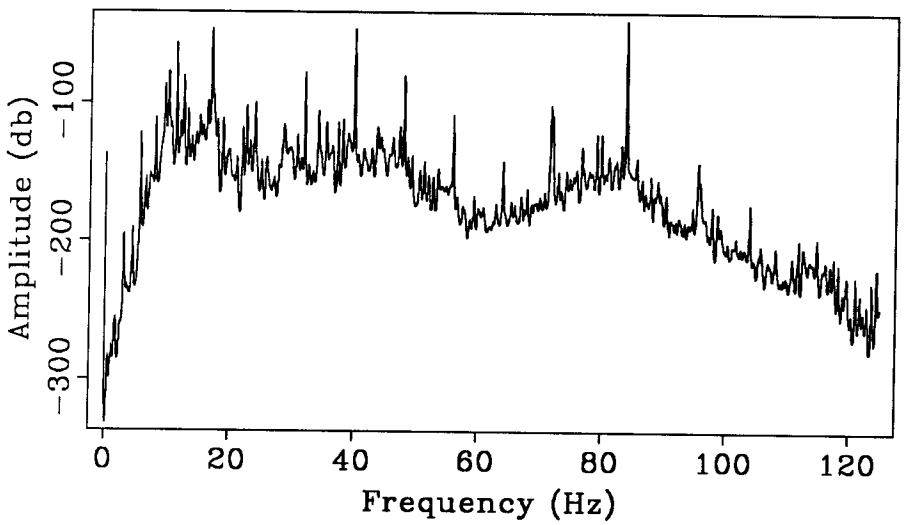

FIG. 4. Spectrum of drill bit data. Average of the spectra of the 30 traces within a gather. The spectra are computed by applying Burg's algorithm with 400 poles. The scale is logarithmic, in decibels (db).

Next the spectra of the signal were computed as a function of recording period. Figure 5 displays the spectra for the EW line, while Figure 6 shows the spectra for the NS line. For each gather, i.e. a recording period of 10 sec, there is one trace in the corresponding figure, obtained as the average of the spectra for each of the 30 traces. Burg's algorithm, with 400 poles, was used in the spectral estimation. The time elapsed between successive gathers is not known.

The spectra of the data from the two lines of geophones are nearly identical. There is a remarkable continuity between the strong spectral lines from one gather to the next. This continuity reveals very clearly the presence of several families of harmonics. Most apparent are the two families with lines at: (1) 8.,16.,24...Hz, and (2) 48.,72.,96.,120. Hz. These families of harmonics correspond most likely to surface equipment, since they appear unrelated to the change in depth of the tool from 56 to 80 m, that occurs at about the 50^{th} gather. If these harmonics correspond indeed to surface sources, typically with velocities less than 1 km/sec, the signal recorded at the array is most likely aliased in space, (Figure 2).

Variations of spectral lines with time

In this section we apply methods for analysis of time-variable narrow-band signals to the drill-bit data. Our goal is to appreciate the variability of the signal over a recording period of 10sec. A time-invariant model is computationally convenient. On the other hand, a time-variable model offers a more detailed description of the signal, and leads to algorithms for filtering or beamforming that have better performance than their time-invariant counterparts.

Figure 7 is an example of a single trace, bandpass-filtered around one of the strongest harmonics at 11.3Hz. The bandwidth of the filter is 3Hz. There are

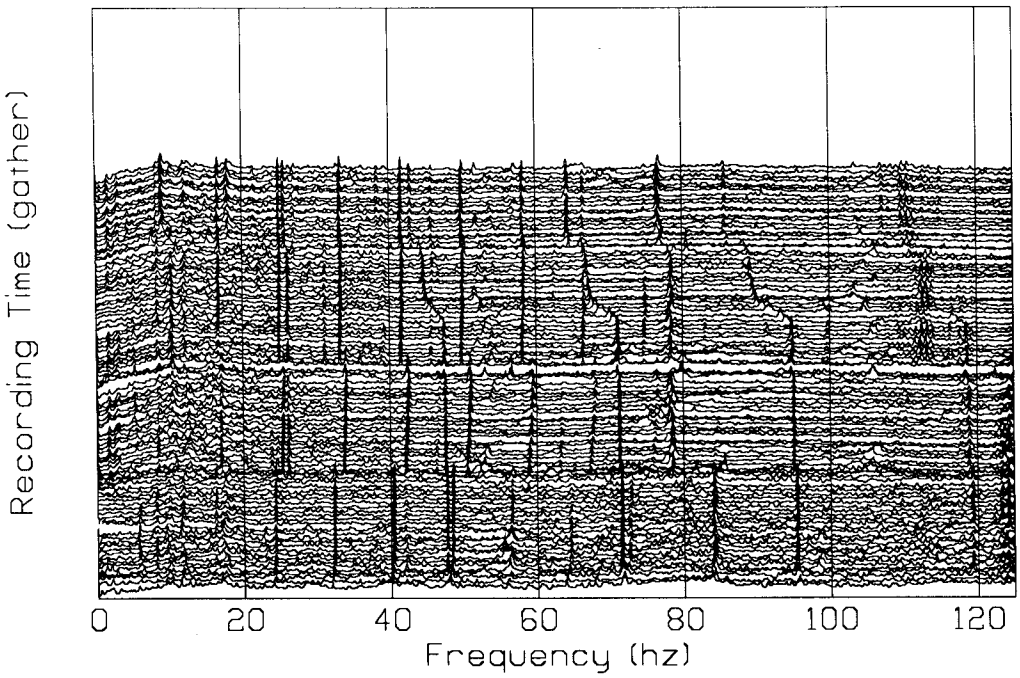

FIG. 5. Spectra for the EW line as a function of recording time. Several families of harmonics are apparent, the strongest being at (1) 8.,16.,24...Hz and (2) 48.,72.,96.,120.Hz.

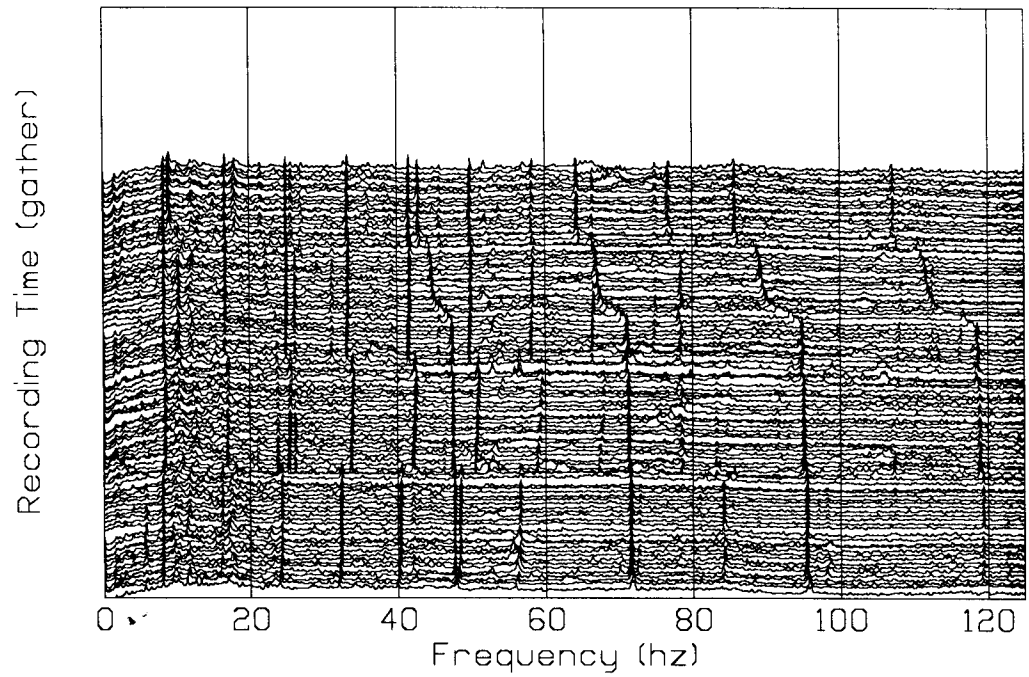

FIG. 6. Spectra for the NS line as a function of recording time. Several families of harmonics are apparent, the strongest being at (1) 8.,16.,24...Hz and (2) 48.,72.,96.,120.Hz. The spectra for the EW (Figure 6) and NS lines are very similar.

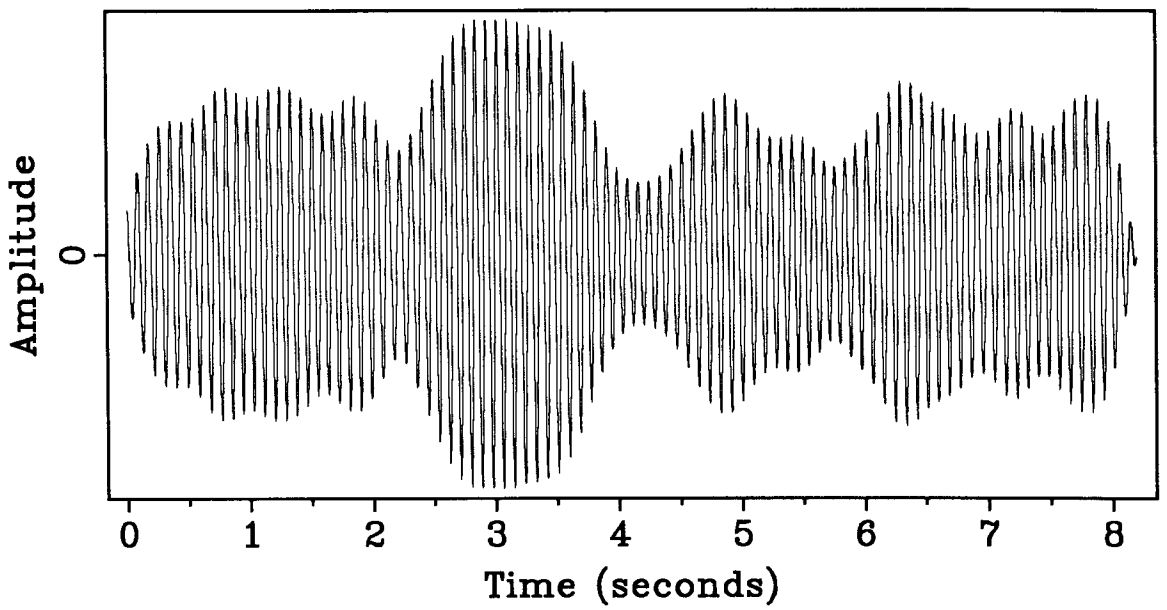

FIG. 7. A single trace, filtered around one of the strongest harmonics (11.3hz) with a 3hz-wide bandpass filter. The signal is approximately sinusoidal but is affected by remarkable variations of amplitude with time.

remarkable variations in the power of the sinusoid; frequency variations, are also present, as shown below (Figures 9 and 10.)

The signal appears as a sinusoid modulated in amplitude and frequency. To determine whether these modulations are due to variations in the characteristics of the source, we examine their consistency from one trace to another. As the spectral lines are organized in families of harmonics, we examine also the coherency between harmonics in one family. The method of analysis is of interest for the description of both the drill-bit signal and the sources of noise at the surface.

Description of the demodulation algorithm

The algorithm that is used to compute the amplitude and the frequency variations for a given single trace is sketched in Figure 8. The selected harmonic is extracted from the original trace s(t) by means of a narrow-band filter, with band wide enough to avoid distortion of the modulated sinusoid and narrow enough to attenuate any adjacent harmonic. A real-valued narrow-band signal can be represented as:

$$A(t)\cos[2\pi f_p t + \phi(t)],$$

where A(t) is the amplitude modulating signal, f_p the nominal value of the harmonic, and ϕ(t) the instantaneous phase as a function of time. Thus, the instantaneous frequency for such a model is given by:

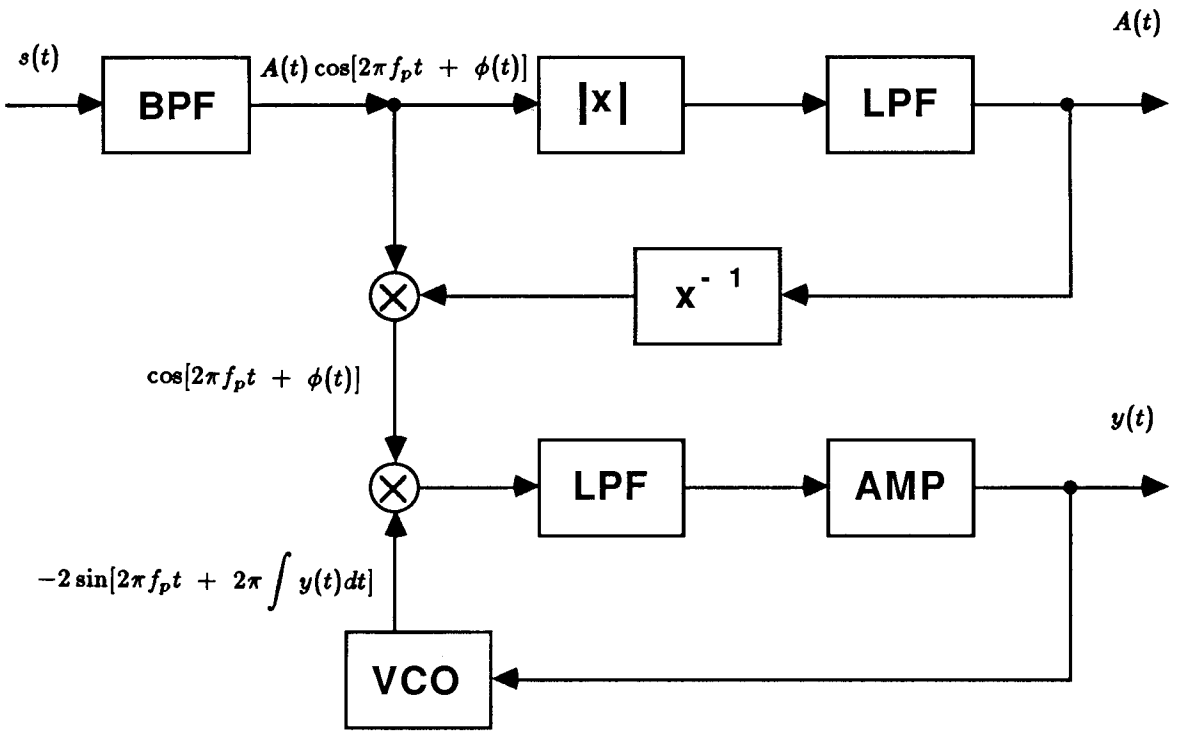

FIG. 8. Block diagram of the processing algorithm used for the analysis of the amplitude and frequency variations of a single harmonic component; s(t) is the original trace recorded at a single receiver. After narrowband filtering at the selected frequency the signal corresponds to an amplitude and frequency modulated sinusoid. The modulus of that signal is extracted and low-pass filtered in order to get the amplitude modulating signal A(t). Dividing the modulated sinusoid by A(t), the amplitude modulation is removed. A Phase-Locked Loop follows, giving as output the driving signal of the variable oscillator; after the lock-in transient, this signal coincides with the instantaneous frequency variations around the nominal value of the harmonic.

$$f_i(t) = f_p + \frac{\phi'(t)}{2\pi}.$$

A simple AM demodulator, which takes the modulus and low-pass filters the incoming signal, is implemented in order to get the instantaneous amplitude A(t). The amplitude modulation is then removed from the original harmonic so that a constant amplitude sinusoid is the input of the Phase-Locked Loop used as a frequency demodulator.

The PLL basically consists of a low-pass filter, an amplifier and a variable oscillator, from now on called VCO (Voltage Controlled Oscillator) following EE traditions. After a lock-in transient, the feedback signal tends to keep the the VCO, originally tuned on the nominal frequency f_p, close to the variable frequency of the input signal.

Without entering into the details of the lock-in procedure, let us see how the PLL can keep the VCO locked. The signal entering the low-pass filter consists of two components, respectively located near the dc and near $2f_p$; the latter is undesired and suppressed by the filter. Actually in our PLL implementation, we insert a notch filter, tuned on twice the frequency of the VCO, in order to remove residual components still present around that frequency. Thus the signal entering the amplifier can be written as:

$$\sin[\phi(t) - 2\pi \int y(t)dt].$$

However, since the VCO is supposed locked, the argument of the sin function, i.e. the phase error, is small and hence the following approximation is valid:

$$\sin[\phi(t) - 2\pi \int y(t)dt] \approx \phi(t) - 2\pi \int y(t)dt.$$

As a result, if G is the gain of the amplifier, the output y(t) is given by:

$$y(t) = G\phi(t) - 2\pi G \int y(t)dt.$$

Deriving and transforming in the frequency domain we get:

$$j2\pi f Y(f) = j2\pi f G\Phi(f) - 2\pi G Y(f),$$

from which:

$$Y(f) = \frac{jf}{1 + \frac{if}{G}}\Phi(f).$$

Thus, if the gain G is sufficiently high:

$$y(t) = \frac{\phi'(t)}{2\pi}.$$

Therefore y(t) is a good approximation of the instantaneous frequency variations of the incoming signal and the VCO frequency can be kept locked.

A more detailed analysis is necessary to understand how the gain of the amplifier and the transfer function of the filter relate first to parameters such as the bandwidth and the damping factor, and second, to the stability of the PLL and its behavior during the lock-in transient (Best, 1984.) Here it is sufficient to say that the parameters of our PLL have been adjusted to guarantee a bandwidth of 3hz with a damping factor of about 0.7.

Data examples

Figures 9 and 10 show respectively the instantaneous amplitude A(t) and the instantaneous frequency variations y(t), resulting from the application of the algorithm to one gather recorded on the E-W line; the selected harmonics (11.3 and 17 hz) belong to the same family; they are multiples of 5.66hz.

The signals A(t) and y(t) remain virtually unchanged from one trace to another except for a delay in time depending only on the position of the trace. For harmonics from the same family, one expects to find amplitudes and center frequencies that are coherent in time. Therefore, the crosscorrelation between the amplitude functions A(t) estimated for 11.3hz and 17hz was computed at one single receiver (Figure 9c). Similarly Figure 10c shows the crosscorrelation between the frequency variations.

In both cases, the crosscorrelations show maxima which confirm the expected coherency, even though they are broader than expected, reminding that the crosscorrelation of finite sequences decays according to the length of the overlapping time window.

The maximum of the crosscorrelation in Figure 10c is not exactly at zero lag. This could be an indication of dispersion; further confirmation of dispersion is given by the velocity analysis discussed below. It is not clear why the same effect is not observed for the crosscorrelation function of the instantaneous amplitude A(t).

In conclusion, these results demonstrate the variability in time of the signal and suggest that further processing should be time-variant.

ANALYSIS OF SPATIAL-COHERENCY

In this section, we apply three different methods to the problem of estimating parameters describing the wavefront of a narrow-band signal. This is a preliminary to the filtering, either for attenuation or for enhancement of a particular wavefront.

A narrow-band signal $s(t)$, recorded at a receiver at location $\mathbf{x}$, can be represented as function of time t, in the following way:

$$s(t,\mathbf{x}) = A(t,\mathbf{x})e^{j\omega\tau(t,\mathbf{x})}e^{-j\omega t},$$

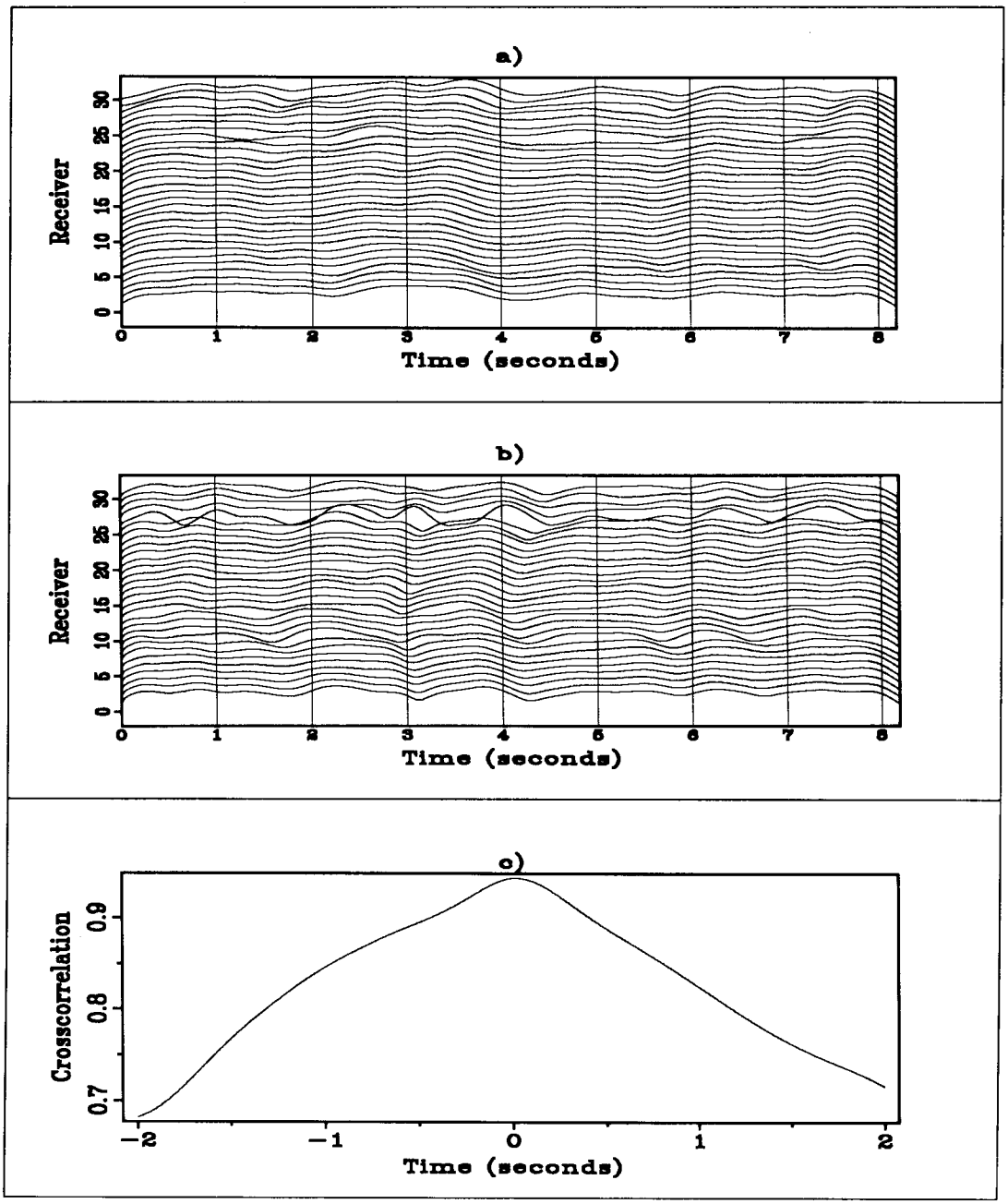

FIG. 9. Analysis of amplitude variations with time for different harmonics and receiver positions. The amplitude variations are computed according to the scheme of Figure 8. a) Amplitude versus time for the harmonic centered at 11.3hz and for each receiver of the E-W line. b) Amplitude versus time for the harmonic centered at 17hz and for each receiver of the E-W line. c) Crosscorrelation between the amplitudes variations of the two harmonics observed at one selected receiver. The consistency indicated by the crosscorrelation was expected since the two harmonics belong to the same family (i.e. multiples of 5.66hz.) The relative amplitude variations of the two harmonics are consistent from trace to trace.

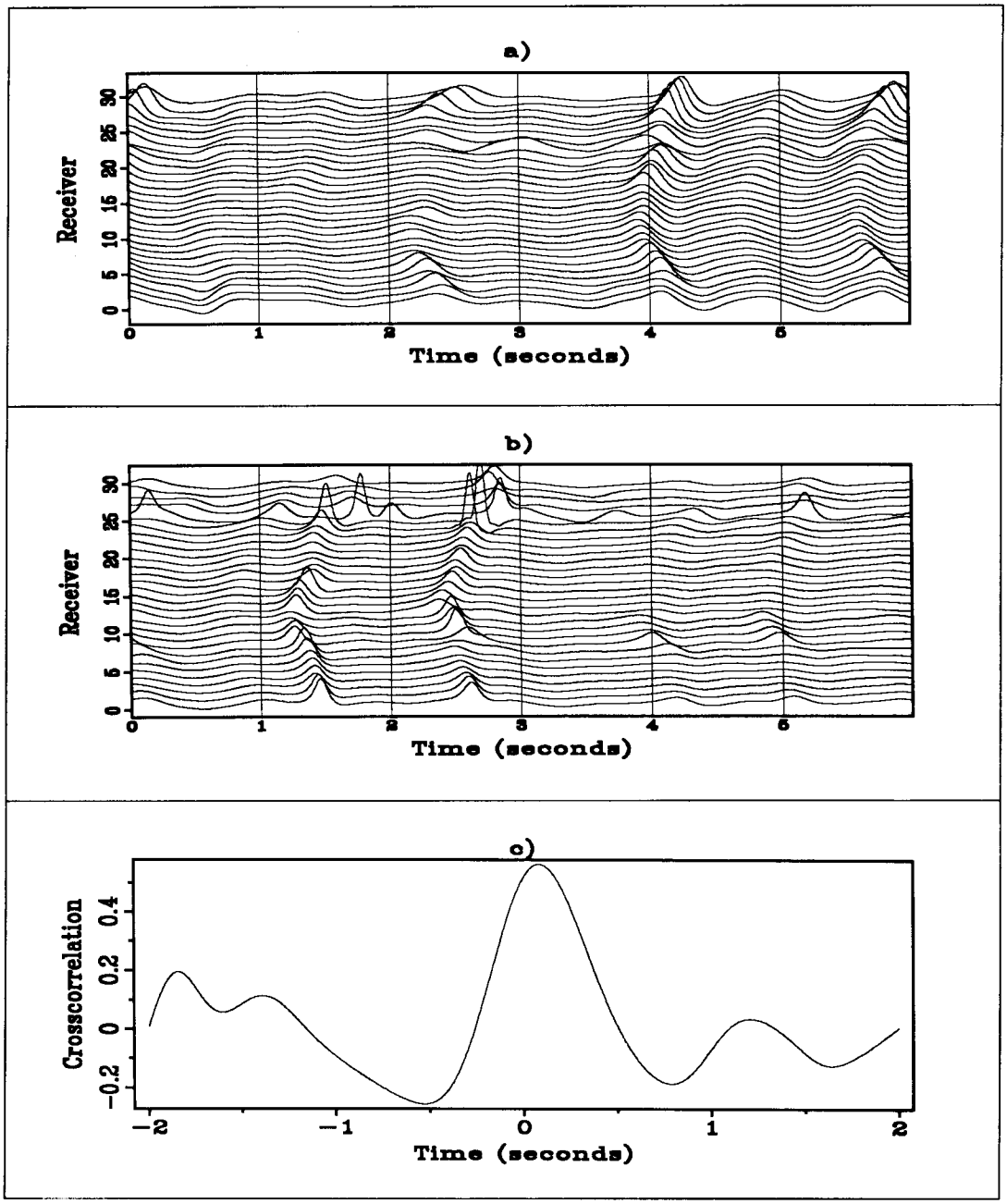

FIG. 10. Analysis of frequency variations with time for different harmonics and receiver positions. The frequency variations are computed according to the scheme of Figure 8. a) Frequency versus time for the harmonic centered at 11.3hz and for each receiver of the E-W line. b) Frequency versus time for the harmonic centered at 17hz and for each receiver of the E-W line. c) Crosscorrelation between the frequency variations of the two harmonics observed at one selected receiver. The crosscorrelation indicates some consistency in the variations of the two harmonics away from the nominal frequency. The maximum of the crosscorrelation function is not exactly at zero which might be an indication of dispersion.

where the central frequency is ω, and $A(t,\mathbf{x})$ and $\omega\tau(t,\mathbf{x})$ are the instantaneous amplitude and phase of the signal. For monochromatic signal the instantaneous amplitude and phase are independent of time. When the signal impinging on the array is a plane wave, the instantaneous phase is linear in $\mathbf{x}$. Instead, for the wavefront generated by a point source located at $\mathbf{x_0}$ in a medium of constant velocity v, the instantaneous phase in the far-field is proportional to the distance between the source and the receiver,

$$\tau(\mathbf{x}) = \|\mathbf{x} - \mathbf{x_0}\|/\mathbf{v}.$$

For the drill-bit data, the curvature of the wavefield across the array is significant, and we choose therefore to model the sources as point-sources.

Interactive velocity analysis

The first method is conceptually the simplest one. However, it relies on the availability of a high-resolution graphics workstation, such as our SUN-3 workstations.

An interactive program, using the SUNVIEW graphics library, reads in input two gathers of data, recorded at the same time. A frequency is chosen from the control panel, Figure 11, then the data are bandpassed and displayed. The coherency pattern appears clearly on both gathers. The signal-to-noise ratio is high, and there is no amplitude modulation along offset as would be expected for interfering signals of comparable amplitudes. The coherency pattern can be related to the parameters describing a point source – two space coordinates along the surface, x_0, y_0, depth z_0, and velocity v_0 – by fitting a hyperbolic curve, computed by taking into account the coordinates of the geophones, and displayed in the style of Jon Claerbout's Overlay program (SEP-51).

Figure 11 shows the best fitting hyperbolas, and their parameters – source located at the head of the well, velocity of the medium equal to 0.65 km/s – for data in the frequency band of width 1Hz, centered at 5.65 Hz. Figure 12 displays the data in the frequency band of width 1Hz centered at 11.3Hz. Again the source is located at the well-head, but this time the best-fitting velocity is 0.55 km/s. The velocity analysis for the harmonic at 16.95 Hz, is presented below using another method, and yields essentially the same result as the one for the 11.3Hz band. This interesting example of velocity dispersion could be attributed either to diffraction – lower frequencies have a greater Fresnel zone and are sensitive to high velocity variations at greater depth than high frequencies – or, to dispersive surface waves.

An example of surface waves is shown in Figure 13. The frequency band is centered at 8Hz. There is a change of polarity of 180° degrees on opposite sides of the well, as expected for Rayleigh waves. No parameters were found that give a good fit of the hyperbola to the moveout of the data.

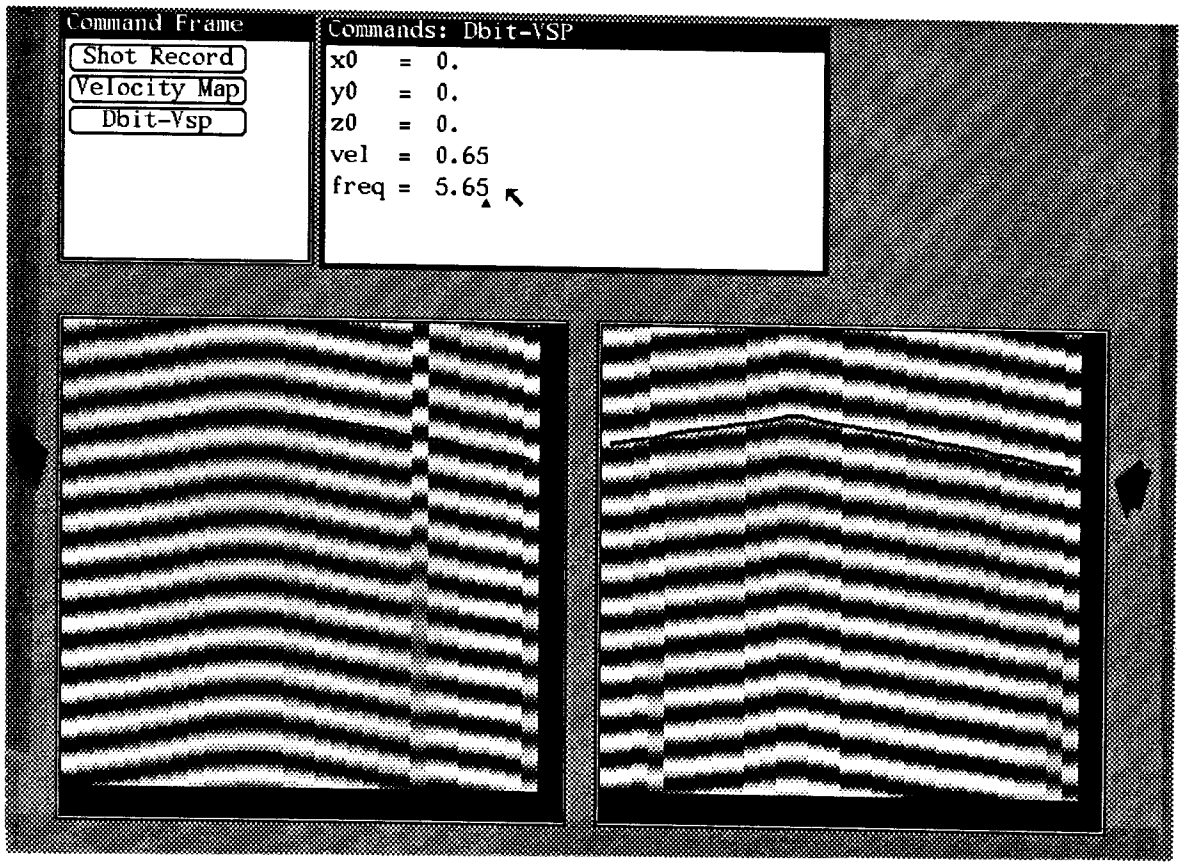

FIG. 11. Frequency band 5.64 Hz. The panel labeled "Commands Dbit-VSP" displays the parameters chosen for the hyperbolas that best fit the moveout of the data. The hyperbolas overlayed on the data are indicated by arrows.

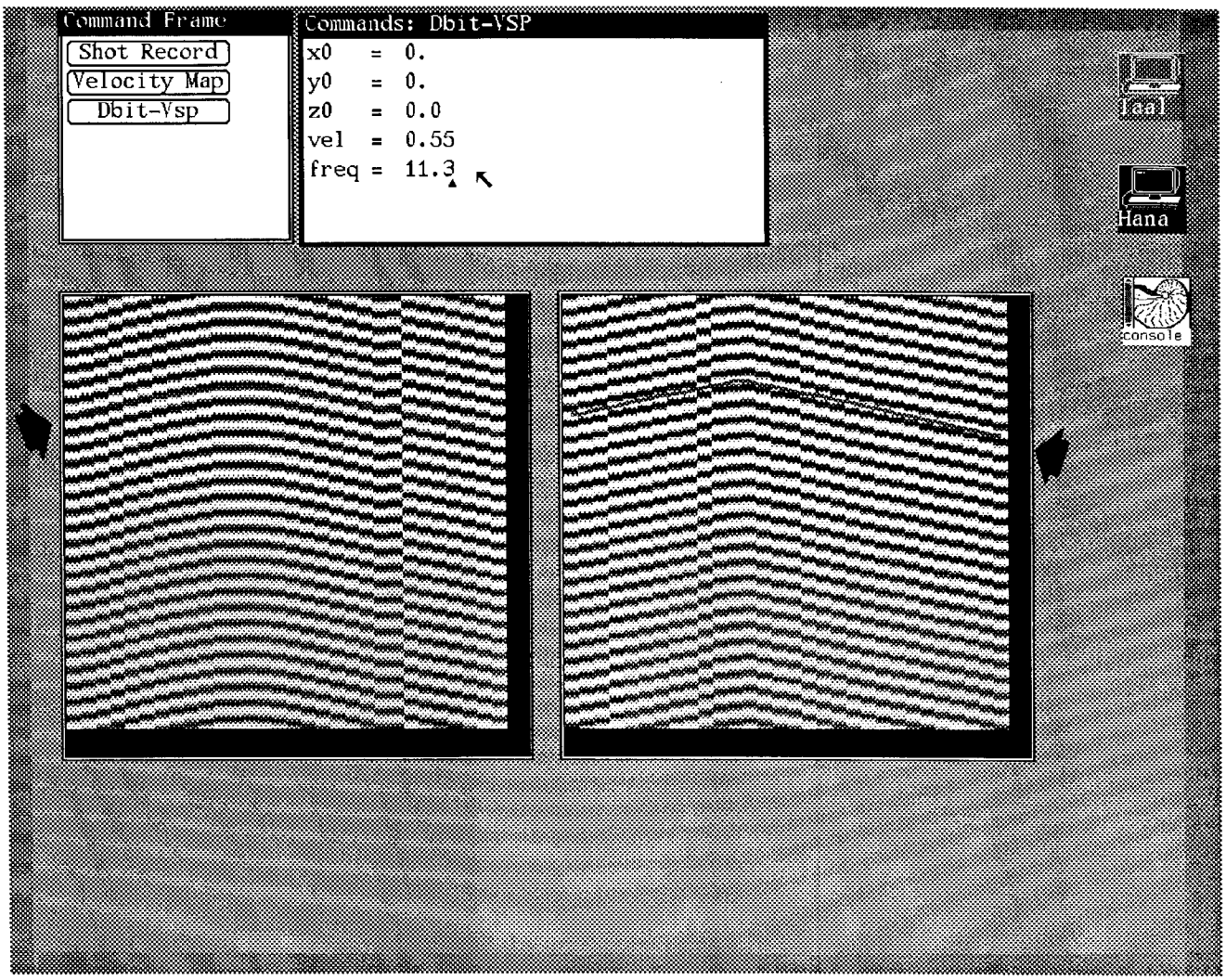

FIG. 12. Frequency band 11.3 Hz. The panel labeled "Commands Dbit-VSP" displays the parameters choosen for the hyperbolas that best fit the moveout of the data. The hyperbolas overlayed on the data are indicated by arrows.

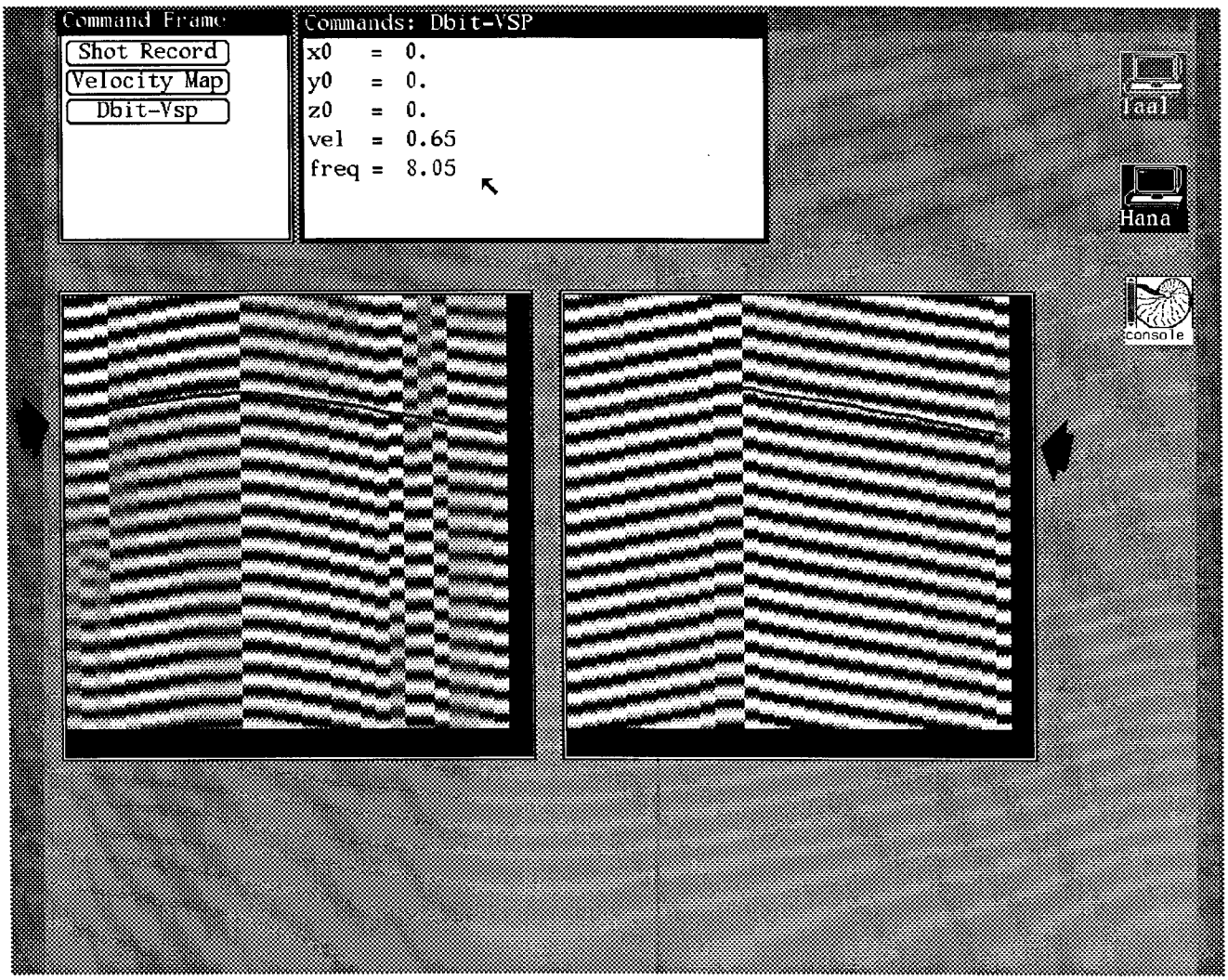

FIG. 13. Frequency band 8.0 Hz. The panel labeled "Commands Dbit-VSP" displays the parameters choosen for the hyperbolas that best fit the moveout of the data. Note the 180° change of phase from one side of the well to the other. The hyperbolas overlayed on the data are indicated by arrows; no parameters were found that allow a good fit.

Estimation of relative phase-shifts

An alternative way to describe the moveout of the harmonics is to estimate their relative phase-shifts as a function of the receivers distances.

Let us assume for a while that $s_1(t)$ and $s_2(t)$ are two monochromatic signals which oscillate at the same frequency and with amplitudes normalized to 1. The relative phase-shift $\Delta\phi$ between the two harmonics can be computed from the following formula:

$$\cos(\Delta\phi) = \frac{2}{T}\int_T s_1(t)s_2(t)dt$$

This formula can be applied to our data, provided that the bandpass filter which selects the harmonic is sufficiently narrow and that the amplitude modulation is previously removed. The algorithm is very simple and fast: the computation time is basically the same as that required for estimating the dc component of the crosscorrelation. Thus the time window T over which the integration is performed can be extremely large to make the algorithm as reliable as possible. In our case, the window is about 500 seconds long, i.e. half the total record time, since for such a time the vertical movement of the drill-bit is equal to 6m, and introduces therefore a negligible variation in the phase of the signal.

The results of the estimation of relative phase-shifts for the harmonic centered at 17hz are given in Figure 14. Four phase curves are plotted according to differences in the position of the drill-bit and the orientation of the recording line. The phases are computed with respect to a couple of reference receivers, one for each side of the cross, which in the case are the nearest to the well. As a result the phase-shifts exceed 360°, and make phase unwrapping necessary. Our phase-unwrapping algorithm is guided by a predefined trend for the phases.

The difference between the phase curves in Figure 14 are related to the differences in position of the two receiver lines with respect to the well. The phase curves seem unsensitive to the change in the depth of the drill-bit from 50m to 85m, thus suggesting that the source is located at the surface. A last remark about Figure 14: the 23^{rd} receiver presents a peculiar misalignment that has not been explained.

In Figures 15 and 16 the same results of Figure 14 are compared with the theoretical phase-shifts estimated on the basis of a model for a monochromatic point source. Depending on the position of the source (surface, 50m or 85m) and on the wave propagation velocity, the synthetical phases lie on different curves; comparing them with the actual data it turns out that the best fitting is obtained assuming a surface point source (Figures 16b and 16c). This happens for both the lines and with the same propagation velocity (580m/s). On the contrary, a good fit could not be obtained for the velocity when assuming a change in the depth of the source. Thus in Figures 15b and 15c, in Figures 13b and 13c, the synthetic

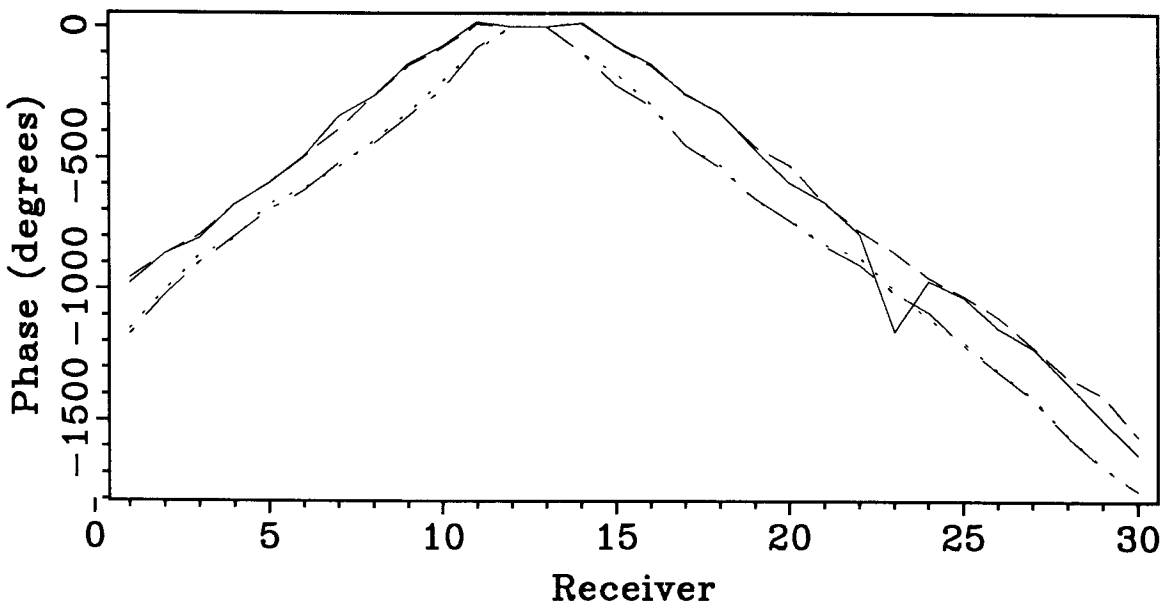

FIG. 14. Relative phase-shifts computed for the harmonic at 17Hz. For each arm of the cross the reference receiver is the nearest to the well location. Four different results are shown according to the following criteria: *(continuous)* east-west line, the drill-bit is at depth 50m; *(dashed)* east-west line, the drill-bit is at depth 85m; *(dotted)* north-south line, the drill-bit is at depth 50m; *(dash-dot)* north-south line, the drill-bit is at depth 85m.

phases are computed for the velocities that separately fit best the actual data with the drill-bit at 50 and 85m.

Stacking velocity analysis

We apply a simple delay-and-sum algorithm to analyze the spatial coherency of narrow-band drill-bit noise. For each choice of source location $\mathbf{x}_0$ and velocity v, we apply a time-delay to the trace at location $\mathbf{x}$ equal to $\| \mathbf{x} - \mathbf{x}_0 \|/v$. Since the trace is narrow-band with central frequency ω, the time-delay involves only a multiplication by $e^{-j\omega \| \mathbf{x} - \mathbf{x}_0 \|/v}$. Then we select the parameters $\mathbf{x}_0$ and v that maximize the power of the stack.

More efficient implementations of this basic algorithm are possible following an analogy with Stolt migration, whereby beamsteering is applied to the plane-wave components of the data, (Cole, SEP-57). On the other hand, if several point sources interfere in a given frequency band, high-resolution methods for velocity analysis could be applied (Biondi and Kostov, SEP-57).

Figure 17 shows a contour map of an array representing the stacking power for the drill-noise data bandpassed at 5.64Hz. The maximum stacking power is obtained for a position of the source at the surface.

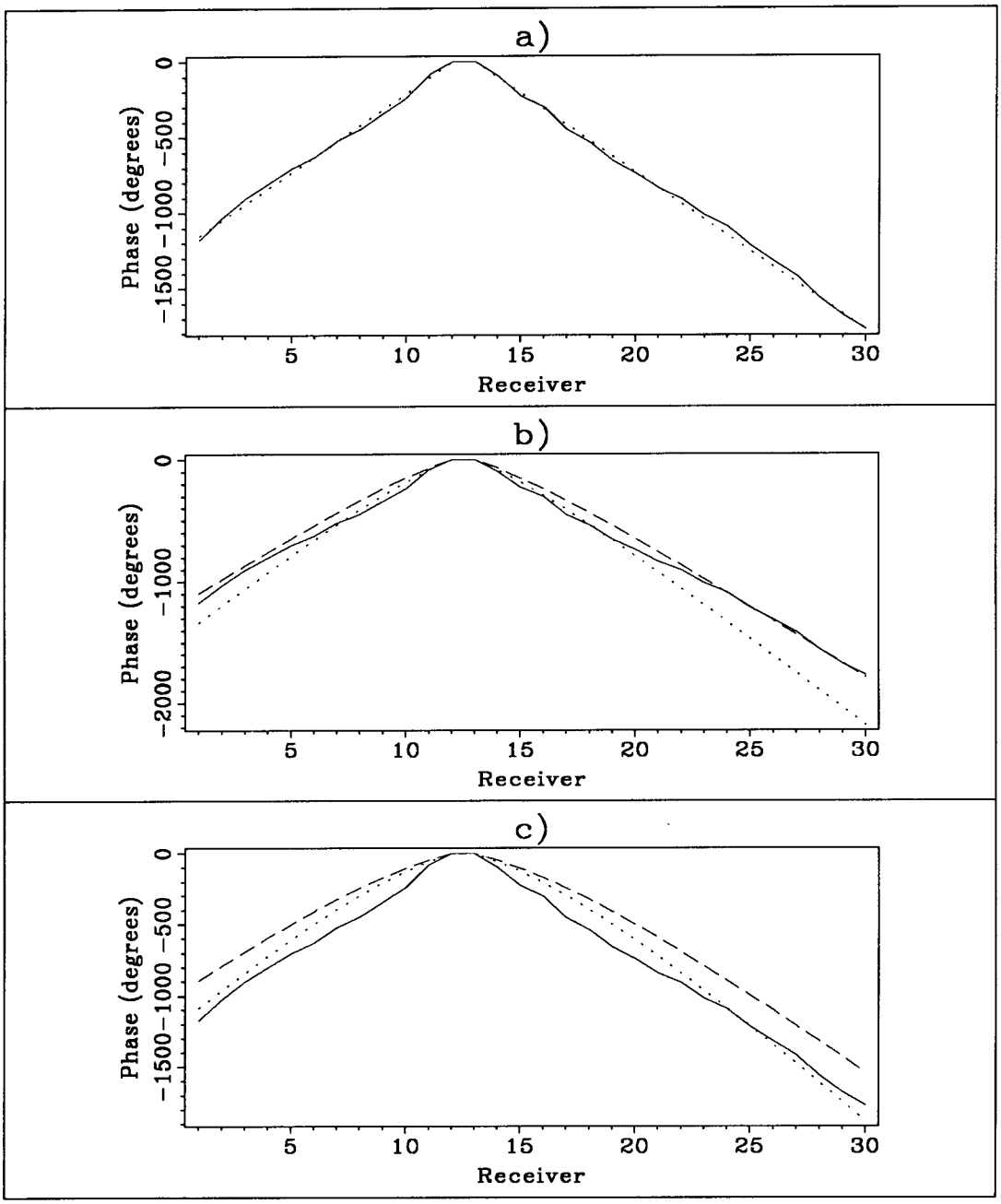

FIG. 15. Relative phase-shifts for the north-south line (continuos line) compared to different theoretical phase-shifts (dashed or dotted lines), based on a model for a monochromatic point source with frequency 17hz. The parameters defining the theoretical phase-shift curves are the depth of the source and the wave propagation velocity. a) Source at the surface; velocity of 580m/s. b) Source at depth of 50m; velocity of 500m/s (dashed curve) or 410m/s (dotted curve). c) Source at depth of 85m; velocity of 500m/s (dashed curve) or 410m/s (dotted curve). The sensitivity of the phase-shifts to the depth of the source is sufficient to stress the impression that this harmonic comes from a surface source. The model fits well the actual data only in a), whereas in b) and c) it is impossible to find a unique velocity value which leads to a satisfactory matching between synthetic and actual data.

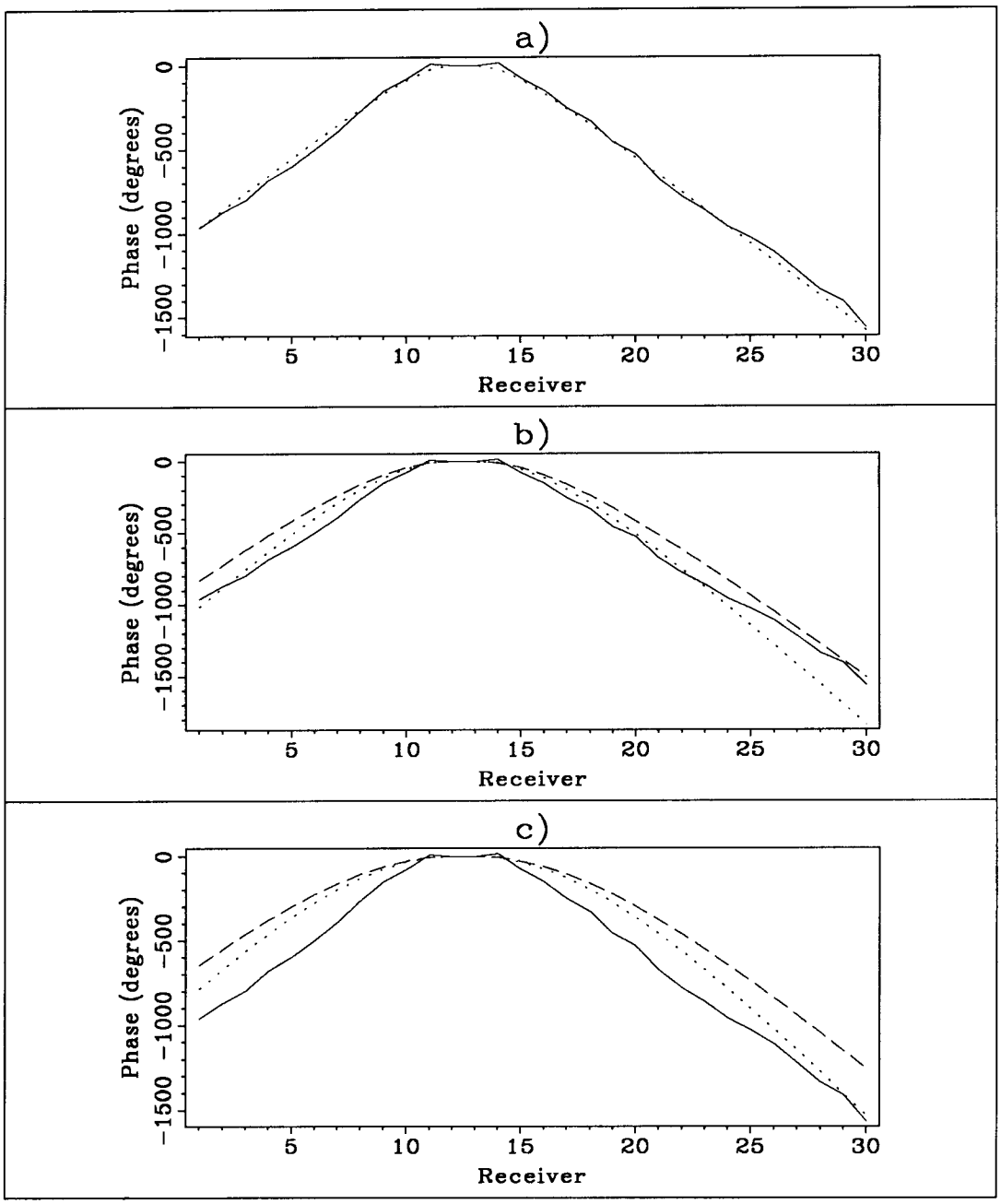

FIG. 16. Relative phase-shifts for the east-west line (continuous line) compared to different theoretical phase-shifts (dashed or dotted lines), based on the model as specified for Figure 15. a) Source at the surface; velocity of 580m/s. b) Source at depth of 50m; velocity of 500m/s (dashed curve) or 410m/s (dotted curve). c) Source at depth of 85m; velocity of 500m/s (dashed curve) or 410m/s (dotted curve). The results are very consistent with Figure 15: again the model fits well the actual data only in a) and the best fitting velocity is the same.

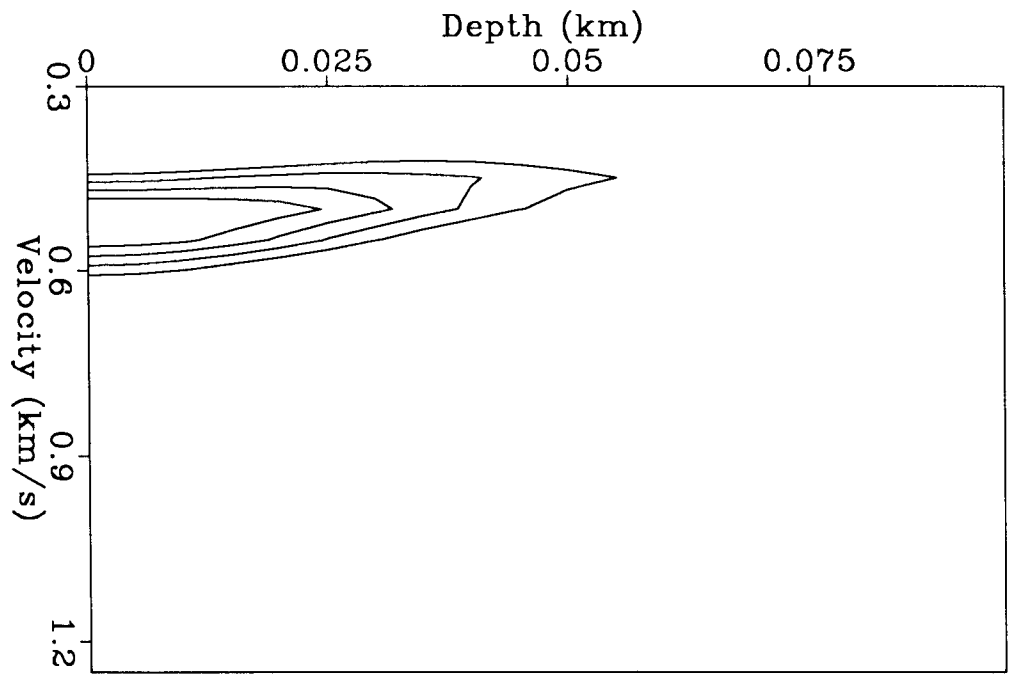

FIG. 17. Contour map of the power for one gather of drill-bit noise bandpassed at 11.64Hz. The maximum of the stack occurs for a position of the source at depth zero, that is at the well-head.

Figure 18 shows the velocity spectra for drill-noise data bandpassed at 5.64Hz and at 11.3Hz. The position of the source is at the well-head. The velocities corresponding to the maxima of the stack agree with the previous two methods of velocity analysis.

CONCLUSION

Our work with drill-noise data from a field survey shows the importance of strong, narrow-band sources. We described methods to track changes in time of the characteristics of spectral lines, and to locate sources in space. Applied to the data from a shallow-well survey, these methods allowed us to identify a point source at the head of the well and surface waves.

Our next goal is to apply similar techniques to identify arrivals from the drill-bit, as well as reflections, in data from survey conducted at deeper wells.

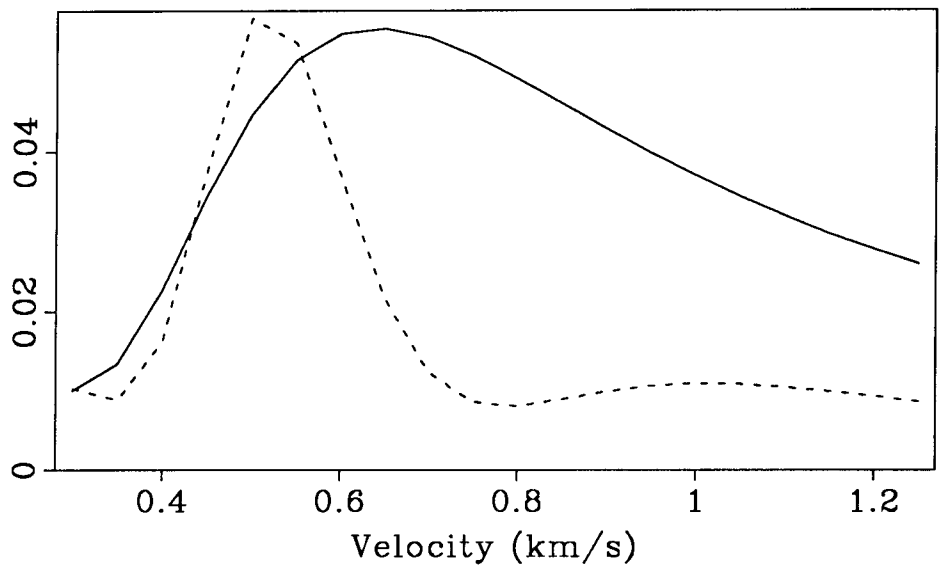

FIG. 18. Velocity spectra for a source located at the well-head. The velocities found by the stacking method agree with those found previously.

ACKNOWLEDGMENTS

We would like to thank Fabio Rocca for communicating to us his enthusiasm about the drill-noise project, as well as for many helpful ideas.

One of us (C.K.) would like to thank Jakob Haldorsen from GECO and Douglas Miller from Schlumberger-Doll Research for many interesting discussions of the drill-noise experiment.

Our thanks go also to the Osservatorio Geofisico Sperimentale (OGS) in Trieste for making the data from the shallow-well survey available to SEP students.

REFERENCES

Best, R.E., 1984, Phase-locked loops: McGraw-Hill, Inc. .

Biondi, B., and Kostov, C., 1988, High-resolution velocity spectra using eigenstructure methods: SEP–**57**.

Cassano, E., and Rocca, F., Multichannel linear filters for optimal rejection of multiple reflections: Geophysics, **38**, 1053–1061.

Claerbout, J.F., 1987, Interpretation with the Overlay program: SEP–**51**.

Claerbout, J.F., 1985, Fundamentals of geophysical data processing: Blackwell Scientific Publications.

Cole, S., 1988, Examination of a passive seismic data set using beam-steering: SEP–**57**.

Harlan, W., Claerbout, J.F., and Rocca, F., 1984, Signal/noise separation and velocity estimation: Geophysics, **49** , p. 1869 – 1880.

Marple, S.L., 1987, Digital spectral analysis with applications: Prentice-Hall.

Samec, P., and Kostov, C., 1988, Borehole-to-surface wave propagation: modeling with finite elements: SEP–**57**.